Acta Oceanol. Sin., 2022, Vol. 41, No. 5, P. 27–40
https://doi.org/10.1007/s13131-021-1969-x
http://www.aosocean.com
E-mail: ocean2@hyxb.org.cn

Statistical characteristics and mechanisms of mesoscale eddies in the North Indian Ocean

Chunjian Sun[1, 2], Xidong Wang[3], Anmin Zhang[1]*, Lianxin Zhang[2], Caixia Shao[3], Guosong Wang[2, 3]

[1] School of Marine Science and Technology, Tianjin University, Tianjin 300072, China

[2] National Marine Data and Information Service, Tianjin 300171, China

[3] College of Oceanography, Hohai University, Nanjing 210098, China

Received 10 June 2021; accepted 30 September 2021

Abstract

The statistical characteristics and mechanisms of mesoscale eddies in the North Indian Ocean are investigated by adopting multi-sensor satellite data from 1993 to 2019. In the Arabian Sea (AS), seasonal variation of eddy characteristics is remarkable, while the intraseasonal variability caused by planetary waves is crucial in the Bay of Bengal (BOB). Seasonal variation of the eddy kinetic energy (EKE) is distinct along the west boundary of AS, especially in the Somali Current region. In the BOB, larger EKE occurs at the northwest basin from March to May, to the east of Sri Lanka from June to September, and along the east coast of India from November to December. The wind stress work (WW) is further studied to figure out the direct influence of wind forcing on EKE. The WW exerts positive effects on EKE along the west boundary of AS and in the south of India/Sri Lanka during the two monsoon seasons. Besides, the WW also has impact on EKE along the east coast of India in November and December. Eventually, we investigate the characteristics and the driving mechanisms of long lifespan eddies. In the AS, long lifespan anti-cyclonic eddies (AEs) mainly generate in the Socotra, the West Indian Coastal Current and the East Arabian Current regions, while cyclonic eddies (CEs) are concentrated in the northwest region. In the BOB, long lifespan AEs mostly form near the west of Myanmar, while CEs are accumulated at the north and northwest basin. The instabilities caused by Rossby waves, coastal Kelvin waves, seasonal currents, together with wind stress forcing exert enormous efforts on the generation and evolution of these eddies.

Key words: mesoscale eddy, eddy characteristics, North Indian Ocean, satellite altimeter

Citation: Sun Chunjian, Wang Xidong, Zhang Anmin, Zhang Lianxin, Shao Caixia, Wang Guosong. 2022. Statistical characteristics and mechanisms of mesoscale eddies in the North Indian Ocean. Acta Oceanologica Sinica, 41(5): 27–40, doi: 10.1007/s13131-021-1969-x

1 Introduction

Mesoscale eddies with time scales of days to months and spatial scales from dozens to hundreds of kilometers have significant effects on dynamic processes of ocean and atmosphere. More energetic than mean current flow (Morrow et al., 2004), mesoscale eddies can efficiently transport heat, salt and nutrients in the ocean, acting as an active exchange system on the budget of energy and substances (Chelton et al., 2011a; Dong et al., 2014; Hu et al., 2014; Zhang et al., 2014a, b). Besides, mesoscale eddies also exert considerable influences on weather and climate by impacting wind speed, heat fluxes, clouds, rainfalls and typhoons at the air-sea boundary layer (Chelton, 2013; Frenger et al., 2013; Ma et al., 2016; Sun et al., 2020). The advance of high resolution satellite altimeter data greatly improves the accuracy of eddy identification (Chelton et al., 2011b). With the satellite data, mesoscale eddies have been investigated from various aspects over global ocean, such as eddy characteristics, spatial distributions, vertical structures, energy exchanges, transport properties and acoustic structures (Chaigneau et al., 2008, 2009; Chen et al., 2019; Dong et al., 2017; Li et al., 2012; Yang et al., 2013, 2015; Zhang et al., 2016).

Driving by the strong seasonal monsoons, the North Indian Ocean produces distinct mesoscale eddies over the basin. In the west part of the North Indian Ocean–Arabian Sea (AS), distinctive eddies have been spotted in various studies. Bruce et al. (1994) revealed a large anticyclonic eddy (Laccadive High) with center approximately at 10°N, 75°E during the northeast monsoon, and the local and remote wind forcing were regard as the generating mechanism for the eddy. Vic et al. (2014) studied the life cycle of Great Whirl (GW) by adopting ROMS model, whose results confirmed that Rossby waves had important impact on generation and collapse of GW. Prasad and Ikeda (2001) found that a large anticyclonic circulation pattern (Southern Arabian Sea High) appeared in the southern AS during the northeast monsoon, which transported warm and low-salinity water from the eastern AS to the west. Based on sea surface height anomaly (SSHA) data from 1993 to 2003, Al Saafani et al. (2007) suggested that eddies propagated westward at speeds of approximately 6.0 cm/s to 8.5 cm/s in the Gulf of Aden, and the mechanisms for eddy entering into the gulf were attributed to the local Ekman pumping, instability of the Somali Current (SC), and westward propagating Rossby waves. In the east part of the North Indian Ocean, Bay of Bengal (BOB), eddy activities are also distinct. Dandapat and Chakraborty (2016) identified two eddy active zones in the BOB through census study, which located at the offshore of Visakhapatnam and the northern part of western BOB,

Foundation item: The National Key Research and Development Program of China under contract No. 2019YFC1510000; the National Natural Science Foundation of China under contract Nos 41976019 and 41906009.
*Corresponding author, E-mail: anmin.zhang@tju.edu.cn

and the seasonal wind stress curl was responsible for the genesis of these eddies. Chen et al. (2012) studied the statistical features of mesoscale eddies in the BOB from 1993 to 2009, demonstrating that baroclinic instability of the background flow was source of eddy energy. The dominating mechanism of eddy kinetic energy (EKE) was also studied by dividing BOB into four regions. At east of Sri Lanka and western BOB, the EKE was induced by ocean internal instability. However, at the northwest of Sumatra and the coastal rim of the BOB, the effect of wind forcing was as important as ocean internal instability (Chen et al., 2018). Cheng et al. (2013) found that eddy activity was strong in the western and central BOB, while the total eddy energy in the western BOB was higher due to the barotropic/baroclinic instability of mean current. Adopting the reduced gravity model, Cheng et al. (2018) further investigated the dynamics of eddy at central BOB, demonstrating that the coastline geometry of Myanmar bump and Andaman Island, together with the nonlinearity advection were critical for eddy generation.

The Indian Ocean is significantly affected by seasonal counter currents as a result of inverted monsoonal winds (Cai and Li, 2011; Tong et al., 2003), and the monsoons can be mainly divided into two phases in the North Indian Ocean (Fig. 1). During the summer monsoon, strong southwest wind drives Somali Current toward northeast. The anticyclonic GW generates in the SC region, which is induced by Rossby waves and intensified by the retroflection of SC (Vic et al., 2014; Beal and Donohue, 2013). Meanwhile, another anticyclonic eddy named Socotra Eddy generates to the east of Socotra, which is formed after GW collided with the Socotra Island (Fischer et al., 1996; Akuetevi et al., 2016). Along the Omani coast, branches of SC cross the Socotra Island from both sides and merge into the northward East Arabian Current (EAC) (Beal and Donohue, 2013; Fratantoni et al., 2006). Beside the India Peninsula, the West Indian Coastal Current (WICC) flows southward along the west boundary and the East Indian Coastal Current (EICC) flows northward along the east boundary. In the Laccadive Sea, a cyclonic gyre named Laccadive Low exists, which becomes anticyclonic Laccadive High during the winter monsoon. The local and remote wind forcing are supposed to be responsible for the genesis of this eddy (Bruce et al., 1994; Shankar and Shetye, 1997). Near the equator region, the Southwest Monsoon Current flows eastward, transporting high salinity water into the BOB. During the winter monsoon, the Southwest Monsoon Current turns to westward Northeast Monsoon Current, bringing fresh water to the AS (Han and McCreary, 2001). Likewise, the directions of SC, EAC, WICC and EICC also reverse. The currents are weak and unstable during transitional periods between the two monsoon phases (Schott and McCreary, 2001; Shankar et al., 2002). As a result, the characteristics of mesoscale eddies are closely connected with monsoon cycles in the North Indian Ocean.

Aiming to obtain a comprehensive understanding of eddy characteristics and the impacts of alternative monsoons in the North Indian Ocean, this study investigates the statistical characteristics and mechanisms of mesoscale eddies by adopting satellite altimeter data from 1993 to 2019, and gives a comparison of eddy features between AS and BOB (the study coverage is 3°–26°N, 43°–99°E). The remainder of this paper is organized as follows: Section 2 introduces the data and methods used in this paper. Section 3.1 describes the statistical characteristics of eddies, including eddy distribution, lifespan and radius. Section 3.2

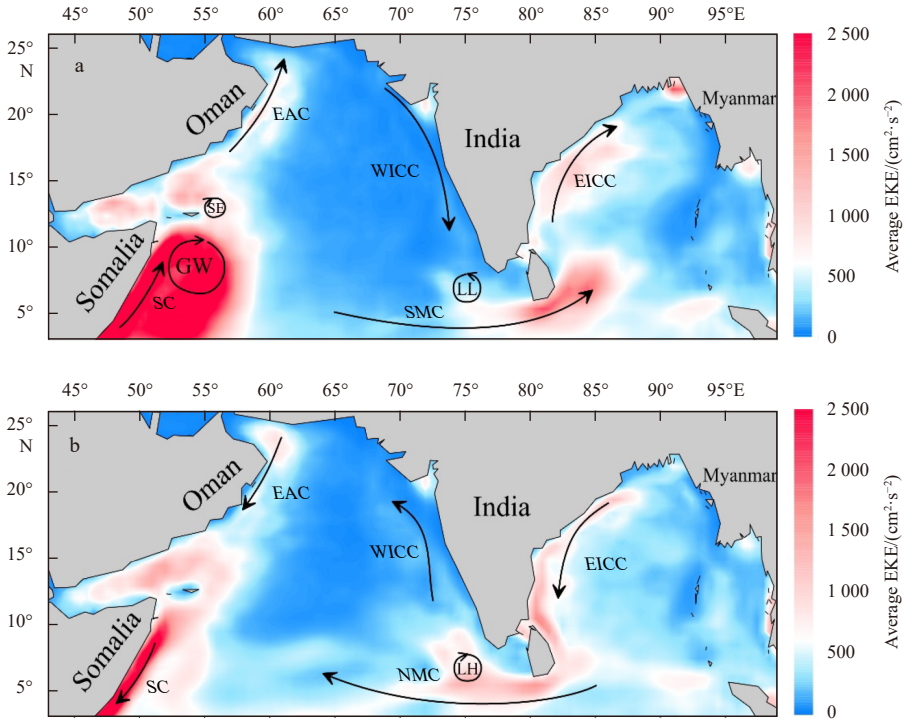

Fig. 1. Schematic currents and surface EKE in the North Indian Ocean during the summer monsoon (a) and winter monsoon (b). The abbreviations are as follows: SC, Somali Current; EAC, East Arabian Current; SMC, Southwest Monsoon Current; NMC, Northeast Monsoon Current; WICC, West India Coastal Current; EICC, East India Coastal Current; GW, Great Whirl; SE, Socotra Eddy; LH (LL), Laccadive High (Laccadive Low). The arrows sketch out the direction of currents and the color shading represents the average EKE in July (a) and January (b).

discusses the seasonal variations of eddy characteristics. The characteristics of long lifespan eddies are further investigated in Section 3.3. Finally, the conclusions are summarized in Section 4.

2 Data and methods

2.1 *Data*

The merged SSHA data are obtained from the Archiving, Validation and Interpretation of Satellite Oceanographic, which have a spatial resolution of 0.25°×0.25° and a daily temporal resolution (Ducet et al., 2000). The wind data are Cross–Calibrated Multi-Platform Version-2.0 from the Remote Sensing Systems with 0.25°×0.25° spatial resolution (Atlas et al., 2011; Wentz et al., 2015). The time coverage is chosen from 1993 to 2019 in this study.

2.2 *Eddy detection and tracking methods*

Satellite altimeter data are capable of identifying signals of mesoscale eddies through various eddy detection methods and promote eddy studies over global ocean (Chelton et al., 2011b). Eddies can be detected from geostrophic flow field calculated from SSHA data by using the Okubo-Weiss method (Okubo, 1970; Weiss, 1991). Moreover, eddies can also be detected from closed geometry curves of SSHA by adopting the Winding-Angle method (Sadarjoen and Post, 1999, 2000). This method calculates closed streamlines by measuring cumulative changes in streamline direction, which is widely used in eddy detection (Chaigneau et al., 2008, 2009). We also adopt the Winding-Angle method in this study. The Winding-Angle method defines an eddy by identifying a point as its center and a series of closed streamlines as contour lines. By searching maximum or minimum values on the SSHA maps, the center of an anticyclonic eddy (AE) or a cyclonic eddy (CE) is identified in a moving window of 5°×5° grid point. Next, the contour lines encircling each AE (CE) center are computed through the streamline following the trajectories of virtual particles released in the geostrophic current field. Finally, the contour lines are clustered to different eddies, and then the entire eddy distribution map is established.

The eddy tracking method suggested by Penven et al. (2005) is applied in this paper. This method defines a non-dimensional distance ($D_{e1,e2}$) as the difference between one eddy (e_1) at time t_1 and another eddy (e_2) at a later time t_2. The distance equation is as follows:

$$D_{e1,e2}=\sqrt{\left(\frac{\Delta D}{D_0}\right)^2+\left(\frac{\Delta R}{R_0}\right)^2+\left(\frac{\Delta\zeta}{\zeta_0}\right)^2+\left(\frac{\Delta \mathrm{EKE}}{\mathrm{EKE}_0}\right)^2}, \quad (1)$$

where ΔD, ΔR, $\Delta\zeta$, and ΔEKE are the spatial distance, radius variation, vorticity variation and kinetic energy variation between e_1 and e_2, respectively. D_0, R_0, ζ_0 and EKE_0 are the characteristic length scale (D_0=100 km), characteristic radius (R_0=50 km), characteristic vorticity (ζ_0=10^{-6} s^{-1}) and characteristic eddy kinetic energy (EKE_0=10^{-2} m^2/s^2), respectively. $D_{e1,e2}$ represents the similarity between e_1 and e_2, and lower value of $D_{e1,e2}$ indicates greater similarity. Thus the algorithm tracks eddies with minimal $D_{e1,e2}$ from t_1 to t_2 as the same eddy. Since eddies mainly move westward, with propagation speed of approximately 10 cm/s according to previous studies (Chaigneau and Pizzaro, 2005), the maximum eastward translational speed is limited to 5 cm/s to avoid inaccurately reversed propagations. Moreover, ΔD is restricted to 150 km to prevent eddy mismatch. The search time interval is limited to two weeks for eddies which may disappear from consecutive SSHA maps when they move to the gaps between satellite tracks, causing interruptions of eddy tracking.

3 Results

3.1 *Eddy statistical characteristics*

Adopting the above mentioned methods, eddies with amplitudes larger than 3 cm, radii greater than 30 km and lifespan more than 10 days are identified in the North Indian Ocean. In total, 2 576 AE (2 378 CE) tracks meet the criteria from 1993 to 2019. Specifically, there are 1 800 AEs and 1 500 CEs in the AS where more AEs yield. In contrast, 776 AEs and 878 CEs generate in the BOB where CEs are relatively numerous. The geographical distributions of eddy numbers counted by the generated positions in 1°×1° box are shown in Fig. 2. Generally, more eddies form at the northwest of AS and north of BOB. In the AS, eddies mainly concentrate along EAC region, which is consistent with the study of Trott et al. (2018). The number of AEs is larger in the GW, Socotra Eddy and Laccadive High regions. Besides, more AEs emerge in the Gulf of Aden than CEs. In the BOB, eddies occur frequently in the north basin or EICC region, similar to result of Chen et al. (2012). CEs tend to concentrate along the north coastline, and yet AEs mainly locate south of these CEs. According to the study of Rao et al. (2010), the north branch of equatorial Kelvin waves propagate anticlockwise along the coastal rim of BOB, causing baroclinic instability and favoring eddy generation. Contrastively, less eddies form in the middle or south sector of AS and BOB. Moreover eddies seldom generate near the equator, where the geostrophic balance is difficult to maintain eddies.

Eddy frequency is defined as the ratio of eddy existing time to total time in the same area (Fig. 3a). Consistent with the distribution of eddy number, the eddy frequency is larger at the west (northwest) part of AS (BOB), where the frequency ranges from 0.4 to 0.8. In contrast, eddy frequency is below 0.3 at the eastern basins, as a result of the low eddy generation rate and short eddy staying time.

The polarity of eddies denotes the probability of an AE or CE vortex in the same region. The expression is as follows:

$$P=\left(F_{\mathrm{AE}}-F_{\mathrm{CE}}\right)/\left(F_{\mathrm{AE}}+F_{\mathrm{CE}}\right), \quad (2)$$

where F_{AE} and F_{CE} are the frequency of AEs and CEs, respectively. When the value of P is positive (negative), the dominant eddy is AE (CE) in the region. The spatial distribution of eddy polarity is featured by bands pattern, varying with latitude (Fig. 3b), which is similar to the results of Yang et al. (2013) in the northwestern subtropical Pacific Ocean. In the AS, a positive band locates between 10°N and 14°N where AEs prevail. Two negative bands reside from 6°N to 10°N and 14°N to 16°N where CEs dominate. These patterns indicate that eddies generally move in zonal direction, as the meridional propagation speed is lower than the zonal speed. However, in the BOB, the propagation of eddies is evidently affected by the north branch of equatorial Kelvin waves along the coastal rim and the Rossby waves radiated from east coast. Therefore, the distribution of polarity is closely related to boundary geometry. A negative band extends along the north boundary, accompanying with a positive band below.

The statistical characteristics of eddy lifespan and radius are shown in Fig. 4. In the AS, approximately 51.8% (41.4%) of AEs (CEs) last longer than 50 days, and about 13.8% (10.5%) AEs (CEs) have lifespan longer than 100 days. Moreover, the percentage of AEs (CEs) longer than 150 days is 3.4% (4.0%). Contrast-

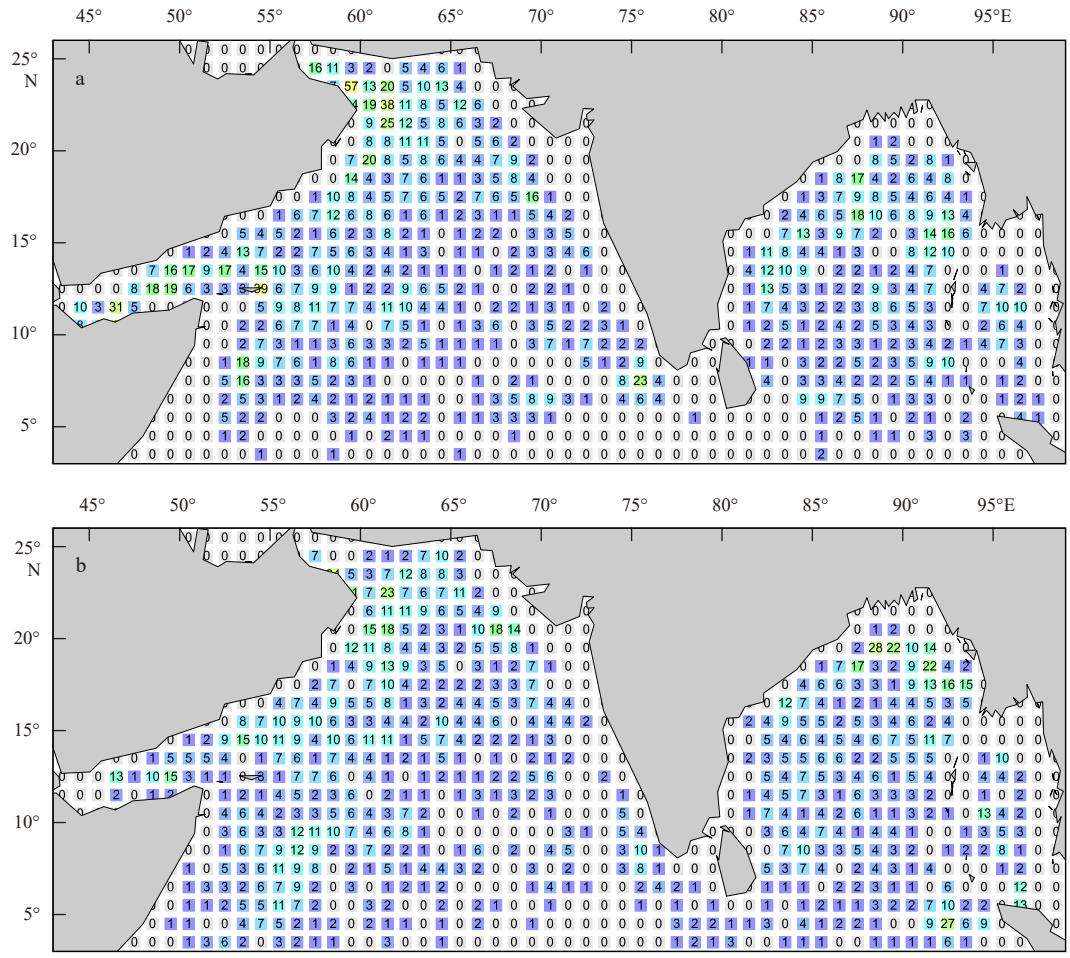

Fig. 2. The distribution of eddy numbers counted by the generated positions in 1°×1° box. a. Anticyclonic eddies, b. cyclonic eddies.

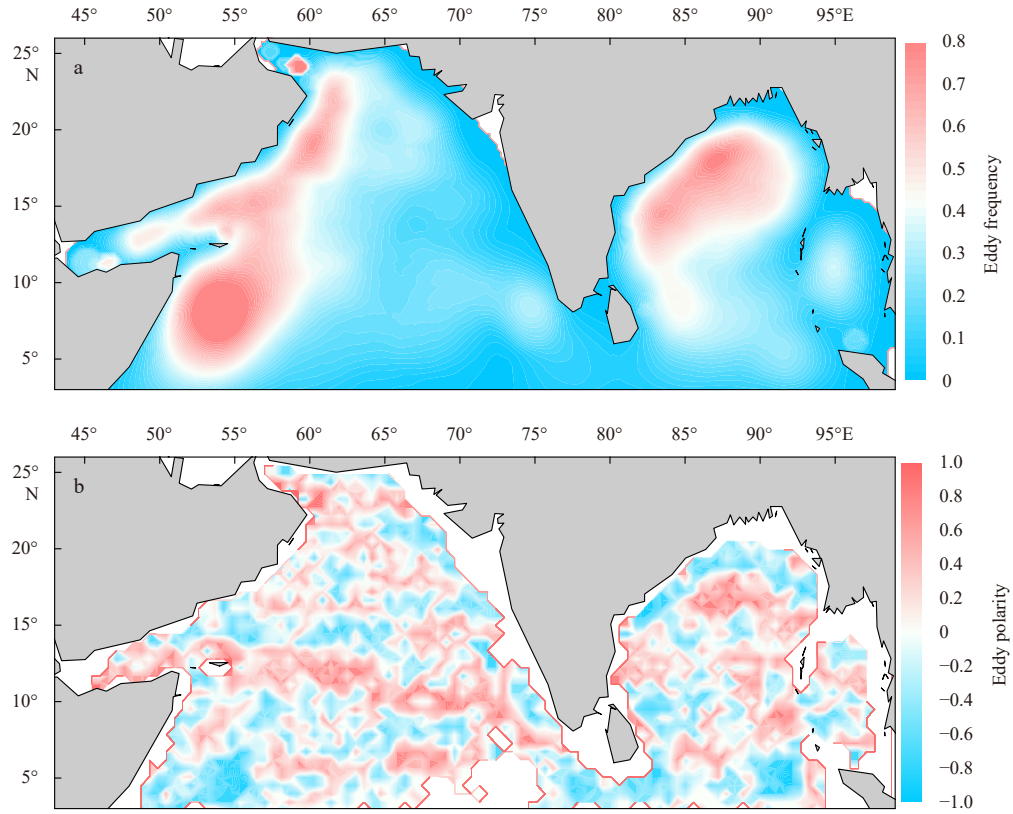

Fig. 3. The distribution of eddy frequency and polarity in the North Indian Ocean. a. Eddy frequency, b. eddy polarity.

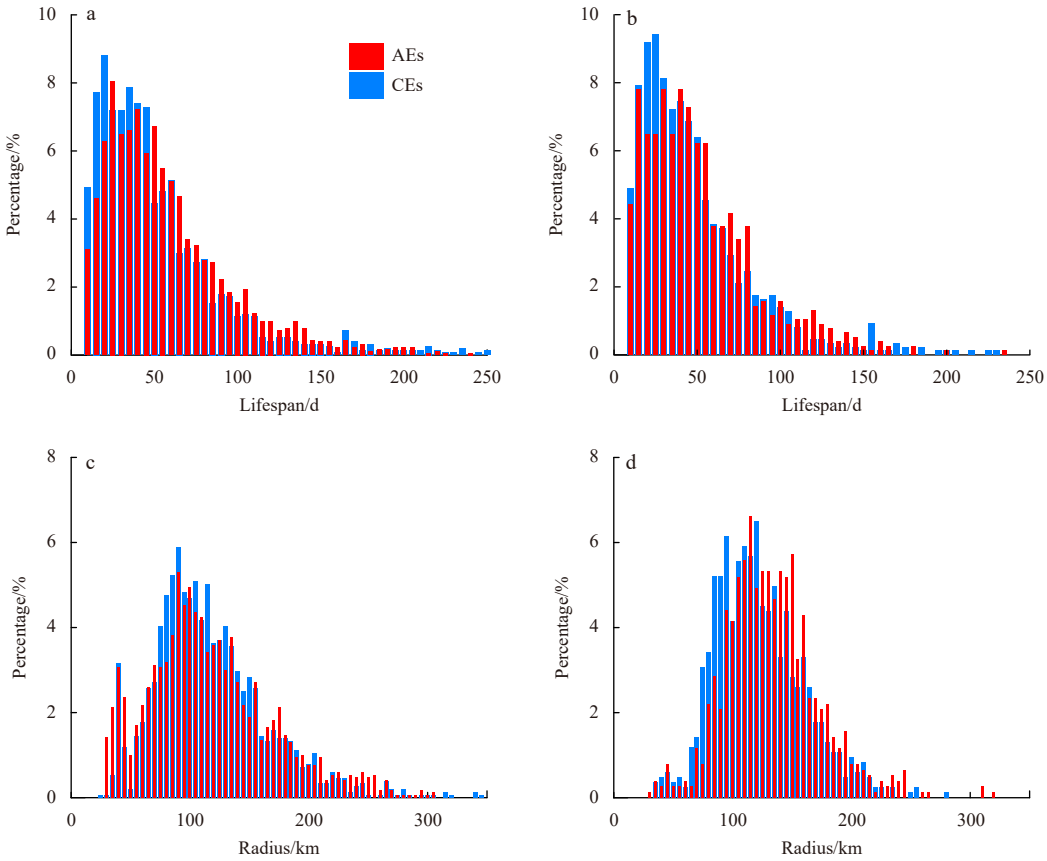

Fig. 4. The proportional histograms of eddy lifespan and average radius during the lifespan. Histogram of lifespan (5-days interval) in the AS (a) and BOB (b), histogram of radius (5 km interval) in the AS (c) and BOB (d).

ively, eddy lifespan is slightly shorter in the BOB, with 45.8% (39.2%), 10.6% (8.5%) and 1.6% AEs (2.8% CEs) surviving more than 50 d, 100 d and 150 d, respectively. The average radii during the lifespan vary from 60 km to 180 km, which account for 72.1% (83.7%) of the AEs (CEs) in the AS, and 12.5% AEs (11.0% CEs) with radii larger than 180 km. In the BOB, the average radii of AEs (CEs) during the lifespan mainly vary from 80 km to 180 km (70 km to 170 km), occupying 85.5% (84.6%) of eddies, similar to the result of Cui et al. (2016). Furthermore, 12.0% AEs and 7.7% CEs have radii larger than 180 km.

From zonal and meridional aspect, the variations of eddy lifespan and radius are further inspected. Figure 5 shows the variations of lifespan with latitude and longitude in the AS and BOB. Eddy lifespan increases with rising latitude and reaches a maximum value at 20°N in the AS. When latitude exceeds 20°N, lifespan starts to reduce as a result of narrowed basin. Similar to AS, the lifespan of eddy in the BOB gradually increases till 16°N. Then, the lifespan of AE decreases, while lifespan of CE still grows from 16°N to 20°N. This is consistent with the negative band of polarity along the north boundary of BOB, indicating these CEs continue to travel along the north boundary. From meridional perspective, lifespan tends to increase from 50°E to 69°E in the AS, and decreases from 70°E to 78°E. Besides, the eddies generated in both west and east region have longer lifespan, which can be identified from the increment at 50°–55°E and 70°–75°E in Fig. 5b. In the BOB, eddy lifespan increases from 82°E to 92°E, and decreases at the remainder segment.

Since the Rossby deformation radius decreases with the rising latitude, the radius of eddy also shows a downtrend with the increasing latitude in both basins (Figs 6a and c). From the longitudinal perspective, the radius of eddy substantially increases from 45°E to 53°E as the basin enlarges. Besides, the radius of eddy has an increment around 75°E, where the LH/LL exist (Fig. 6b). The minimum radius appears at the western boundary of AS where eddies are limited by the narrow Gulf of Aden. In the BOB, the radius of AEs increases at first (Fig. 6d), and then keeps steady from 83°E to 86°E, and gradually decreases from 87°E to 93°E. Comparatively, the radius of CEs is relatively stable from 83°E to 95°E, except for the longitude around 93°E, where radii of both CEs and AEs are compressed due to the scattered Andaman and Nicobar Islands.

Additionally, the zonal propagation speed (u) and meridional propagation speed (v) of eddies are calculated to explore their spatial variations. Positive values refer to eastward and northward. In the AS, u is –8.37 (–8.26) cm/s for AEs (CEs) on average, while it is –8.01 (–8.24) cm/s in the BOB. The absolute value of u decreases as latitude increases (Fig. 7a), which is related to the meridional variation of the Rossby waves phase speed (Willett et al., 2006). From east to west, the absolute value of u generally decreases in both basins (Fig. 7b), demonstrating that eddy propagation speed decreases during the westward propagation process. Compared to the zonal speed, the meridional propagation speed of eddies is much smaller and is southward, with –0.63 (–0.62) cm/s on average for AEs (CEs) in the AS and –0.83 (–0.71) cm/s for AEs (CEs) in the BOB. From latitudinal aspect, v becomes more stabilized with increased latitude (Fig. 7c). From longitudinal aspect, v is more stable at 60°–70°E and 83°–90°E in the central basins (Fig. 7d).

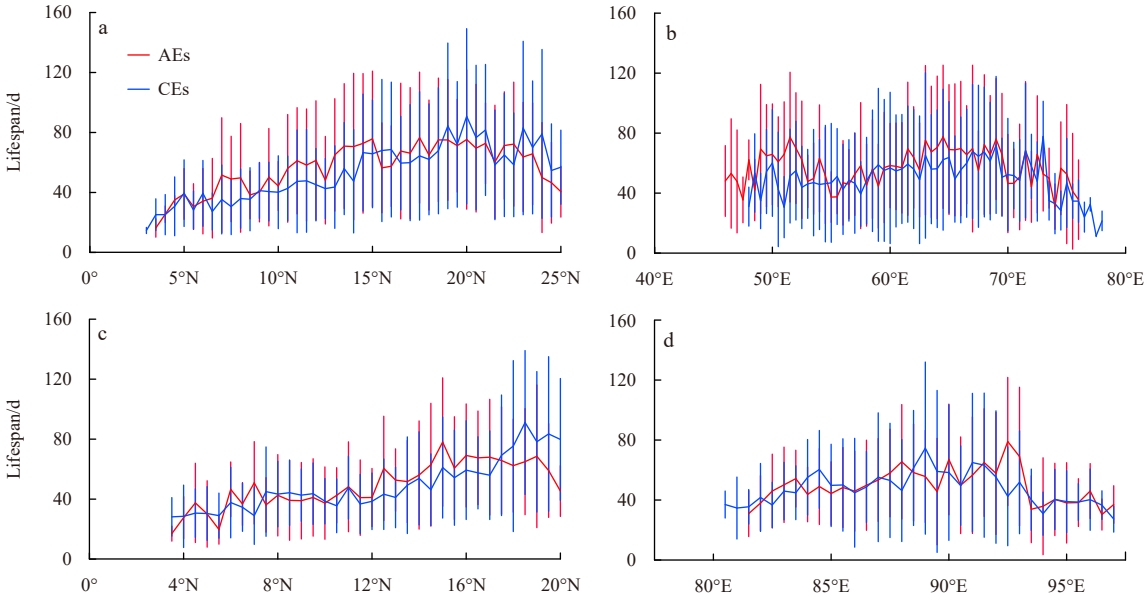

Fig. 5. Lifespan variation with latitude (a) and longitude (b) in the AS, and lifespan variation with latitude (c) and longitude (d) in the BOB. The vertical bars denote the standard deviation of lifespan.

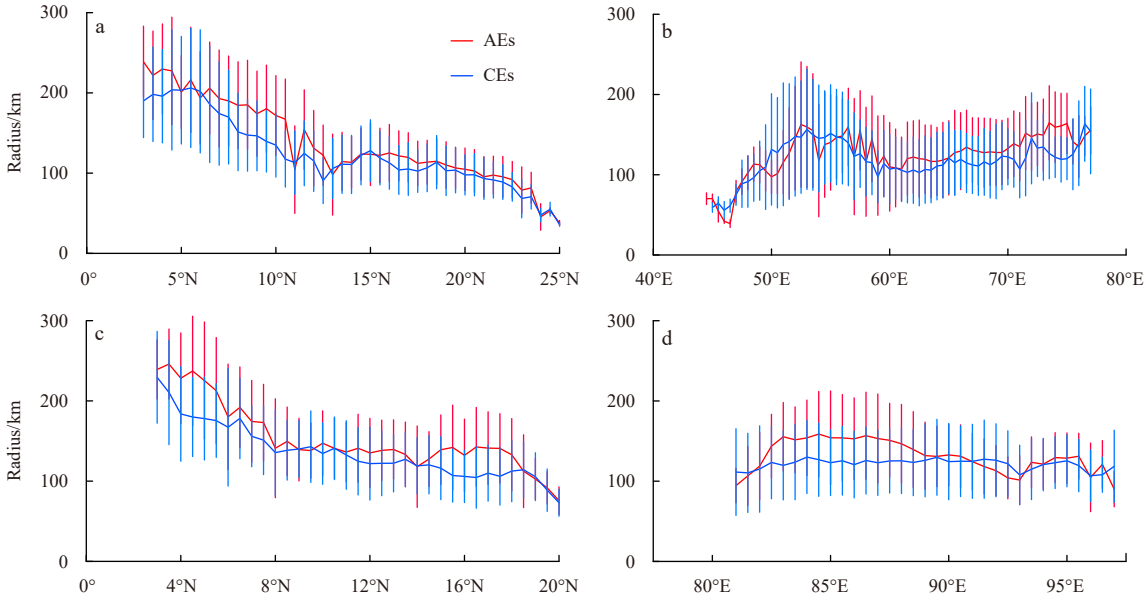

Fig. 6. Radius variation with latitude (a) and longitude (b) in the AS, and radius variation with latitude (c) and longitude (d) in the BOB. The vertical bars denote the standard deviation of radius.

3.2 *Seasonal variations of eddy characteristics*

To study the impact of monsoon cycle on eddy characteristics in the North Indian Ocean, the monthly variations of eddy number, average lifespan, radius and EKE within eddy occupied radius are analyzed. Comparing with other characteristics, the monthly variations of radii are small in both basins, and the radii of AEs (CEs) are slightly larger during the summer (winter) monsoon (Fig. 8c, Fig. 9c).

In the AS, more eddies generate during the winter monsoon, while few eddies emerge during the summer monsoon (Fig. 8a). According to the studies of Rao et al. (2010) and Suresh et al. (2016), the downwelling coastal Kelvin waves propagated across the southern tip of India are further enhanced by the wind stress forcing to the east of Sri Lanka during the winter. Then, the Kelvin waves propagate northward along the west coast of India and radiate Rossby waves into the AS. The instability caused by these waves benefits eddy generation during the winter monsoon period. By contrast, the second upwelling coastal Kelvin waves from BOB could not reach the west coast of India from June to August (Rao et al., 2010) and the upwelling Kelvin waves induced by wind forcing to the east of Sri Lanka cannot fully arrive at the west coast of India until August (Suresh et al., 2016). Moreover, the wind stress of southwest monsoon is intensive and steady (Beal et al., 2013), which continues to supply energy on strong eddies, but produces less perturbation for new eddy generation. Consequently, few eddies form during the summer mon-

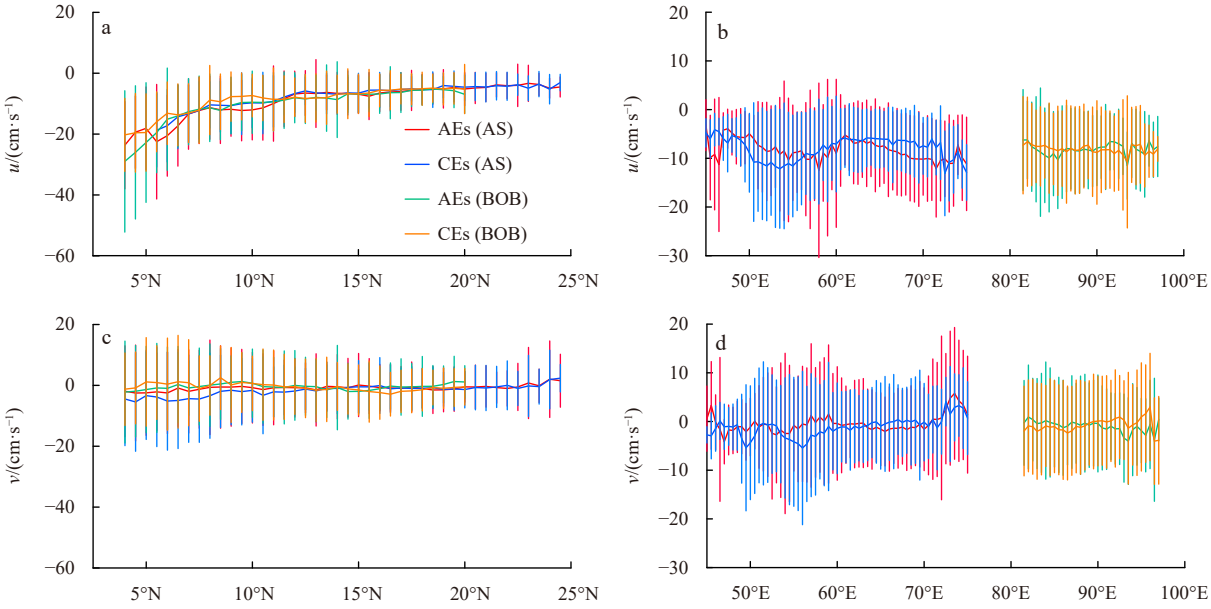

Fig. 7. Variation of u with latitude (a) and longitude (b), and variation of v with latitude (c) and longitude (d). Positive values refer to eastward and northward. The vertical bars denote the standard deviation of u and v.

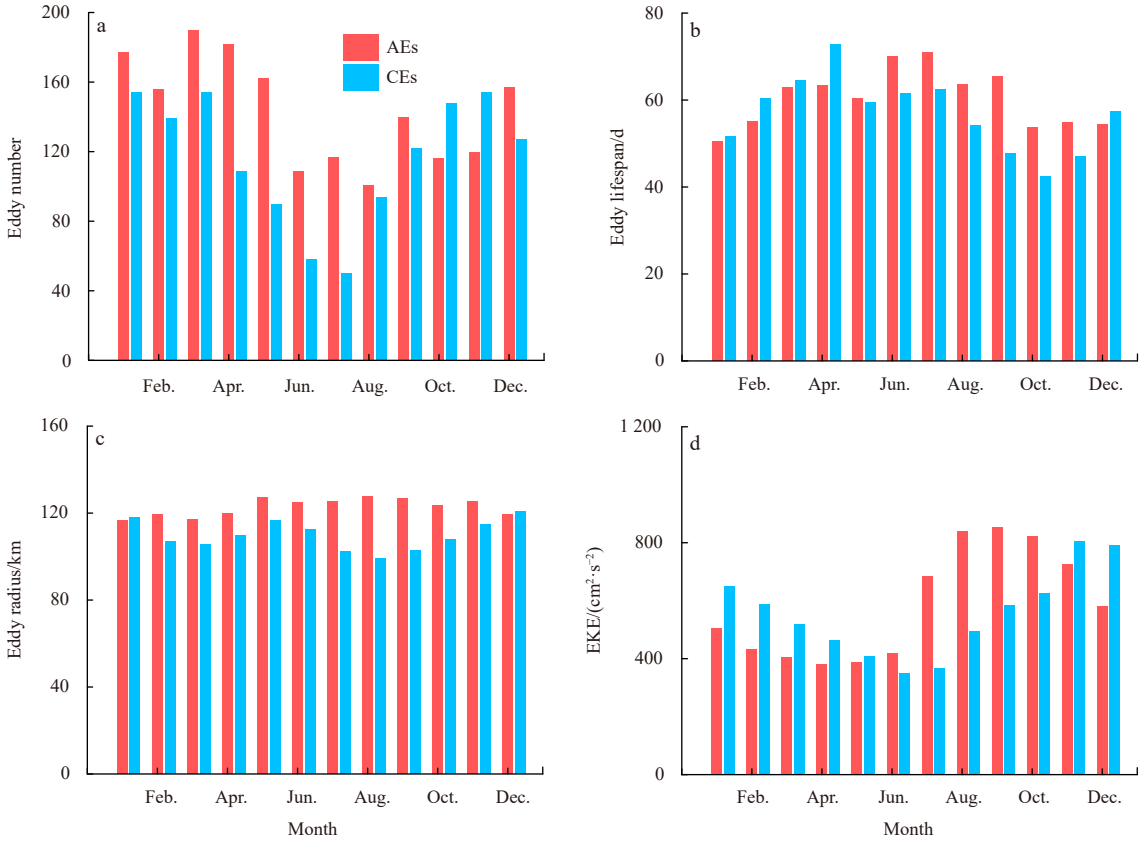

Fig. 8. Monthly variation of eddy characteristics in the AS. a. Eddy number, b. lifespan, c. radius, and d. EKE.

soon. The lifespan and EKE of eddies are affected by seasonal wind and currents. During the summer monsoon, negative wind stress curl dominates, initiating downward Ekman pumping (Mason and Sykes, 1978) and clockwise currents, which are conductive to the enhancement of AEs. As a result, AEs generated before the summer monsoon show an increasing lifespan from January to July and a decreasing lifespan after August (Fig. 8b). The monthly mean EKE of AEs is stronger after July, as the summer monsoon prevails (Fig. 8d). Conversely, positive wind stress curl triggers upward Ekman pumping and anticlockwise currents during the winter, which are beneficial to CEs. Therefore, the lifespan of CEs starts to increase from October before the winter

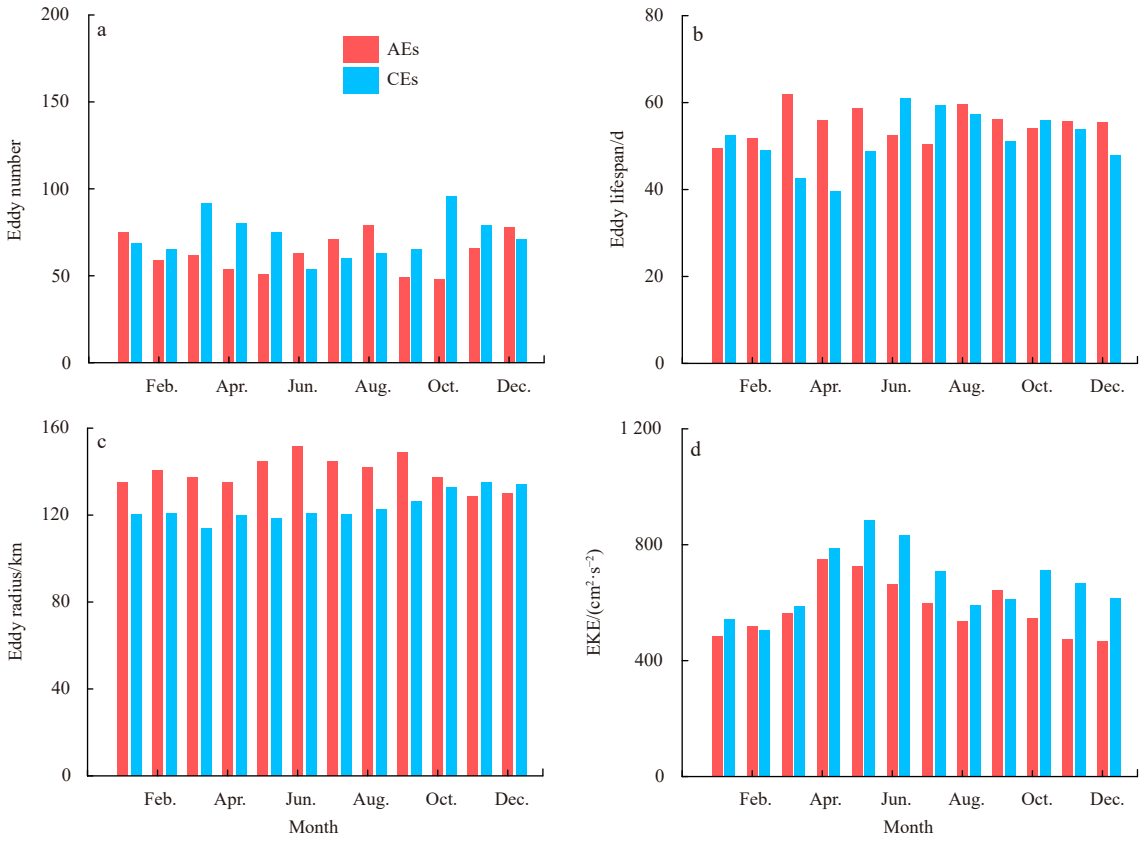

Fig. 9. Monthly variation of eddy characteristics in the BOB. a. Eddy number, b. lifespan, c. radius, and d. EKE.

monsoon, and gradually turns into reduction after May (Fig. 8b). Likewise, the EKE of CEs is larger from November to January during the winter monsoon (Fig. 8d). From geographical aspect, EKE is larger in the SC region, the EAC region and the Gulf of Aden during the summer monsoon (Fig. 10). The instabilities induced by coastal Kelvin waves along the Omani coast (Valsala and Rao, 2016) and west boundary currents could convert kinetic energy of mean flow into EKE in these regions. During the winter monsoon, the area with large EKE in the SC region shrinks, as a result of weakened currents. Besides, the EKE is larger at the Laccadive Sea in winter, which is intensified by the downwelling coastal Kelvin waves across the southern tip of India from November

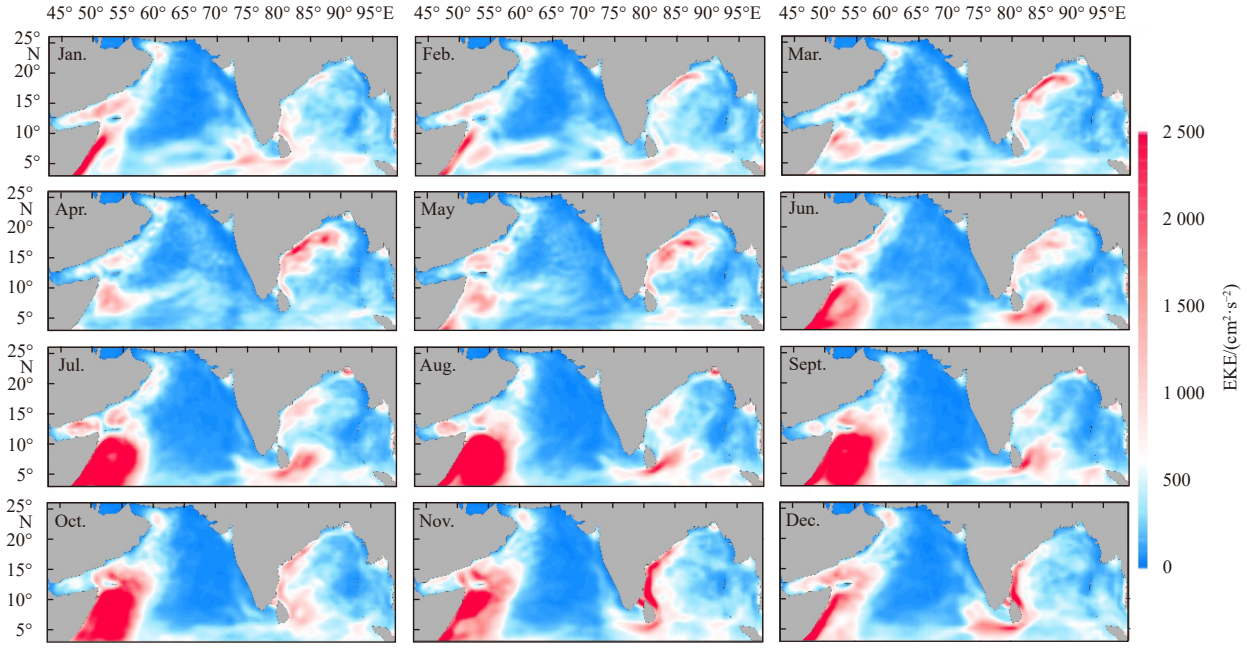

Fig. 10. Horizontal distribution of monthly averaged surface EKE.

(present as positive SSHA in Fig. 11).

In addition to the seasonal wind forcing and currents, the intraseasonal instabilities caused by remote wind forcing and planetary waves also have significant impacts on the variation of eddy characteristics in the BOB (Chen et al., 2018). More CEs generate in February–May and September–November, while more AEs form in June–August and December–January (Fig. 9a). The alternation of upwelling and downwelling Kelvin waves may have influences on the cycle of CEs and AEs generation (Babu et al., 2003; Chatterjee et al., 2017). The monthly variation of eddy lifespan is smaller in the BOB. AEs generated before the arriving of the first downwelling Kelvin waves in March and CEs formed before the arriving of the second upwelling Kelvin waves in June seem to have longer lifespan (Fig. 9b). Unlike AS, the EKE of AEs and CEs in the BOB peaks in April and May, before the summer monsoon onsets (Fig. 9d). During this period, the northeastward EICC flows faster and produces more EKE through instability (Fig. 10). Meanwhile, the first upwelling Kelvin waves (present as negative SSHA along the north boundary of BOB in Fig. 11) and the second downwelling Rossby waves (present as positive SSHA at the western basin of BOB in Fig. 11) radiated from the eastern boundary in pervious year propagate to the northwest BOB during this time (Rao et al., 2010; Sreenivas et al., 2012). The instabilities generated by interaction between these waves and currents further enhance the EKE. From June to September, large EKE occurs to the east of Sri Lanka, which is induced by upwelling Ekman pumping processes of wind stress (Suresh et al., 2016). Moreover, EKE is larger around the east coast of India in November and December, as a result of the instabilities caused by southward EICC and the second downwelling coastal Kelvin waves.

The local and remote wind forcing is crucial to eddies (Chen et al., 2018). The remote wind forcing effects EKE in forms of Kelvin waves and Rossby waves, while the direct contribution of local wind on EKE can be evaluated by wind stress work (WW) (Ivchenko et al., 1997; Zu et al., 2013; Geng et al., 2016), which is defined as:

$$\mathrm{WW} = \left(u'\tau_x' + v'\tau_y'\right)/\rho, \tag{3}$$

where $u'=u-\bar{u}$, $v'=v-\bar{v}$, $\tau_x'=\tau_x-\bar{\tau}_x$, $\tau_y'=\tau_y-\bar{\tau}_y$, $\bar{u}$, $\bar{v}$ and $\bar{\tau}_x$, $\bar{\tau}_y$ denote the mean value of geostrophic velocity and wind stress averaged by the studied time period, respectively.

As shown in Fig. 12, positive WW lasts from June–August and December–February along the west boundary of AS, demonstrating that the wind stress directly impacts on the increment of EKE in these regions during the two monsoon seasons. Comparatively, WW has weaker influence on EKE at the west boundary of BOB during the summer monsoon, whereas the impact of WW is stronger along the east coast of India in November and December. Suresh et al. (2013, 2016) found that the wind forcing around the southern tip of India and east of Sri Lanka had enormous contribution to the sea level at the west coast of India and Laccadive Sea by influencing the coastal Kelvin waves and reflected Rossby waves. Therefore, the wind stress could also enhance the EKE in these regions. During the two monsoon periods, the WW exerts positive effects on EKE around the southern tip of India and southeast of Sri Lanka.

3.3 *Characteristics of long lifespan eddy*

To investigate the characteristics of long lifespan eddies in the North Indian Ocean, eddies with lifespan more than 100 days are further studied in this subsection. Totally, 241 (171) AEs (CEs) in the AS and 78 (64) AEs (CEs) in the BOB are sought out. The corresponding trajectories of these eddies are shown in Fig. 13 with seasonal variation.

In the AS, long lifespan AEs mainly generate in three regions: the Socotra, the WICC and the EAC regions. In the Socotra region, durable AEs are generated at the north and east of Socotra Island from September to December (Figs 13c and d). According to previous studies, AEs are created after GW breaks apart by the Socotra Island during the northward moving process (Akuetevi et

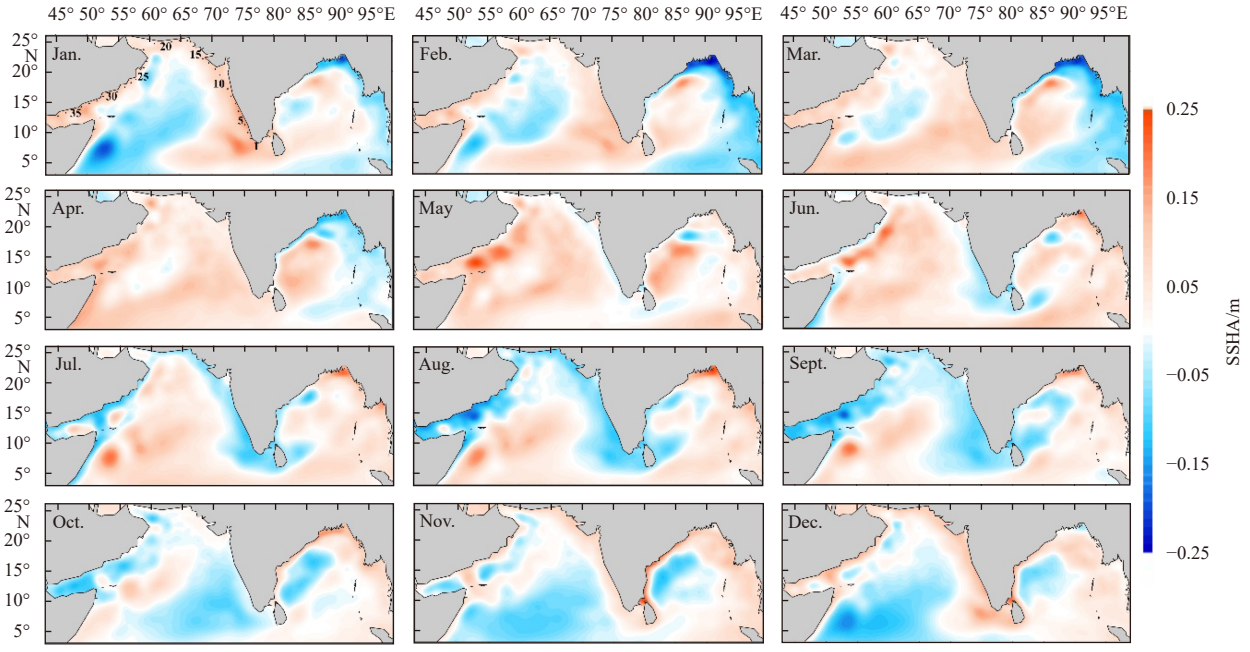

Fig. 11. Horizontal distribution of monthly averaged sea surface height anomaly (SSHA). The numbers in the first subplot mark the positions correspond to the position numbers in Fig. 14b.

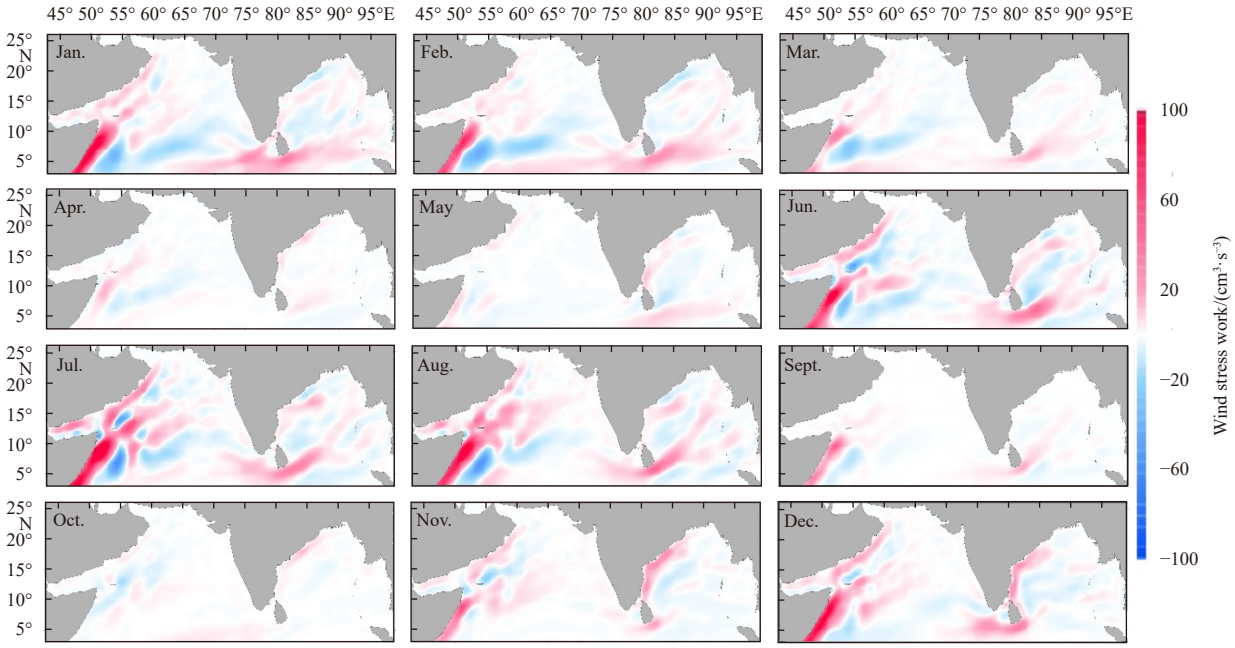

Fig. 12. Horizontal distribution of monthly wind stress work.

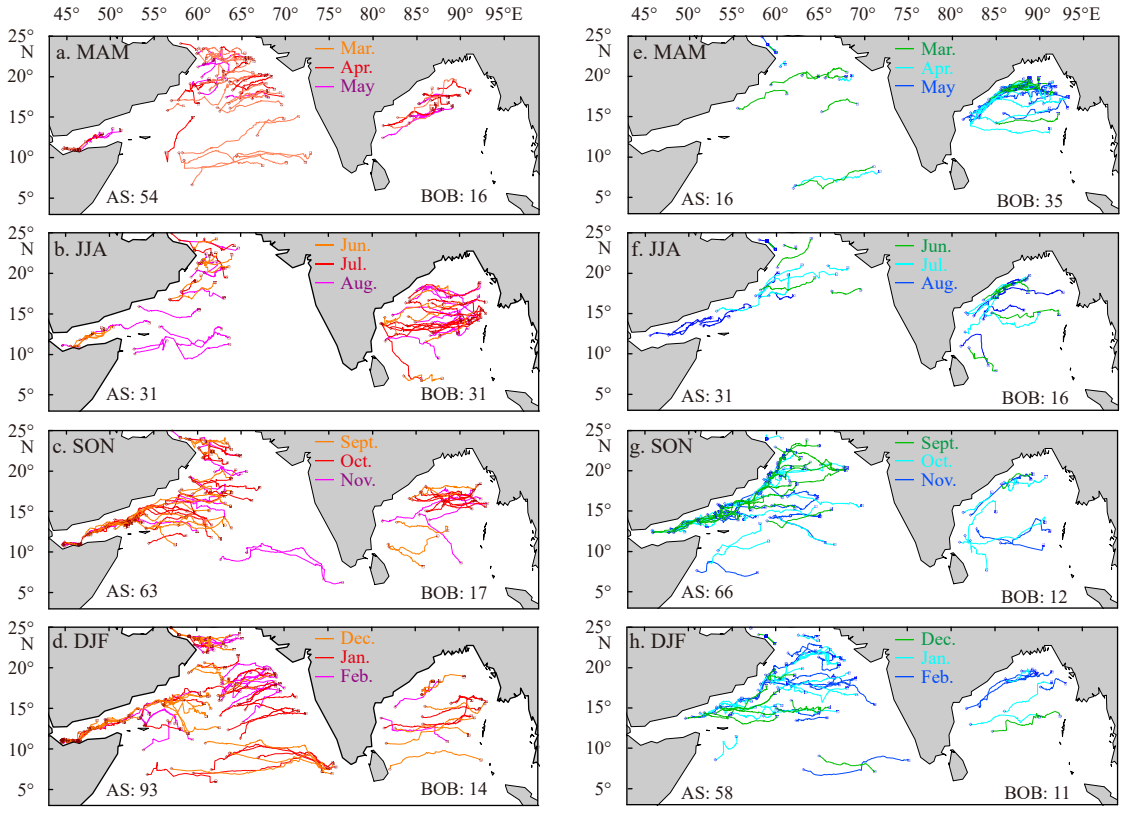

Fig. 13. Trajectories of eddies with lifespan longer than 100 days. a–d: AEs, e–h: CEs. The square symbols denote the generated positions, and the diamond symbols refer to the dissipated positions. MAM, March, April, and May; JJA, June, July, and August; SON, September, October, and November; DJF, December, January, and February; AS, Arabian Sea; BOB, Bay of Bengal.

al., 2016; Fratantoni et al., 2006), which can be regarded as the AEs at north of the Socotra Island. Meanwhile, some of these AEs may propagate into the Gulf of Aden from September to January. The positive WW, together with the westward propagating Rossby waves and coastal Kelvin waves may sustain these AEs (Al Saafani et al., 2007). While the AEs emerged to the east of Socotra Island are triggered by the downwelling Rossby waves radiated from the east boundary of AS since last December, which can be identified from the positive SSHA band (averaged by 10°–15°N) in the time-longitude diagram (Fig. 14a). The characteristics of long

lifespan AEs to the east of Socotra region are further analyzed during normalized evolution process (Fig. 15a). The amplitude raises in the first 70% lifespan, and then it gradually decreases during the rest of lifespan. The trend of EKE is similar to the amplitude. The radius increases in the initiatory 15% lifespan, and decreases during the remaining period. The average WW is 2.48 cm^3/s^3 and the Ekman pumping vertical velocity is -1.10×10^{-6} m/s on average, indicating that both wind stress and downwelling processes contribute to these AEs.

In the WICC region, the location where long lifespan AEs generate gradually pushing northward from December to April (Figs 13a and d), as the downwelling coastal Kelvin waves from BOB propagate northward along west coast of India (show as positive SSHA band in Fig. 14c), simultaneously. The characteristics of these AEs during normalized lifespan are shown in Fig. 15b. The amplitude, radius and EKE have similar trends, which increase at first, and keep stable in 30%–90% lifespan. The average WW is only 0.14 cm^3/s^3, demonstrating that the local wind effect is weak at the east boundary. The Ekman pumping vertical velocity is -0.81×10^{-6} m/s on average. Both Ekman pumping vertical velocity and EKE of these AEs are less than the AEs in the Socotra region, indicating AEs generated in the west basin are much stronger than AEs generated at the east boundary of AS. Additionally, AEs form at the Laccadive High also reveal long lifespan (Figs 13c and d). According to study of Suresh et al. (2016), the downwelling Rossby waves forced by the wind stress to the east

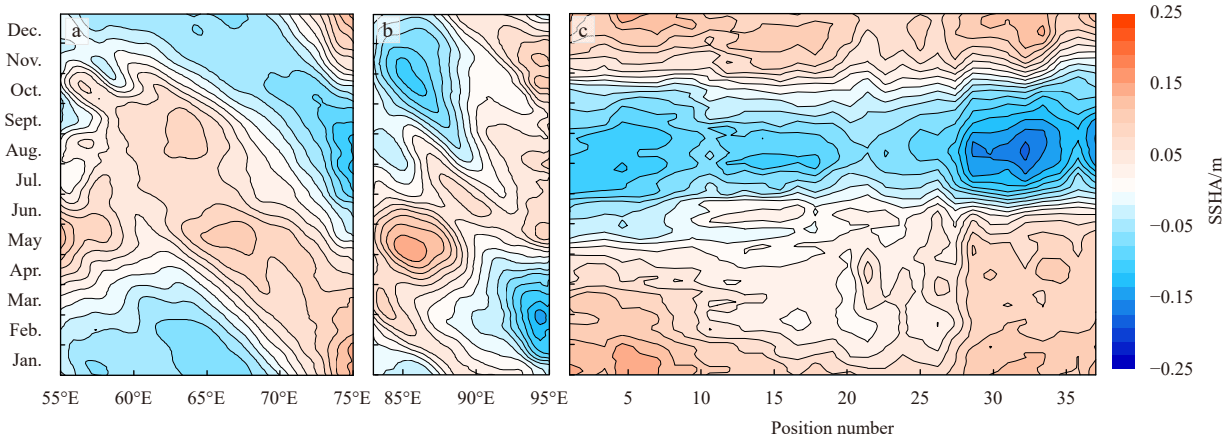

Fig. 14. Time-longitude diagram of multi-year mean annual cycle of SSHA averaged from 10°N to 15°N in the AS (a), averaged from 14°N to18°N in the BOB (b), and SSHA along the north boundary of AS (c). The position numbers are marked in first subplot of Fig. 11.

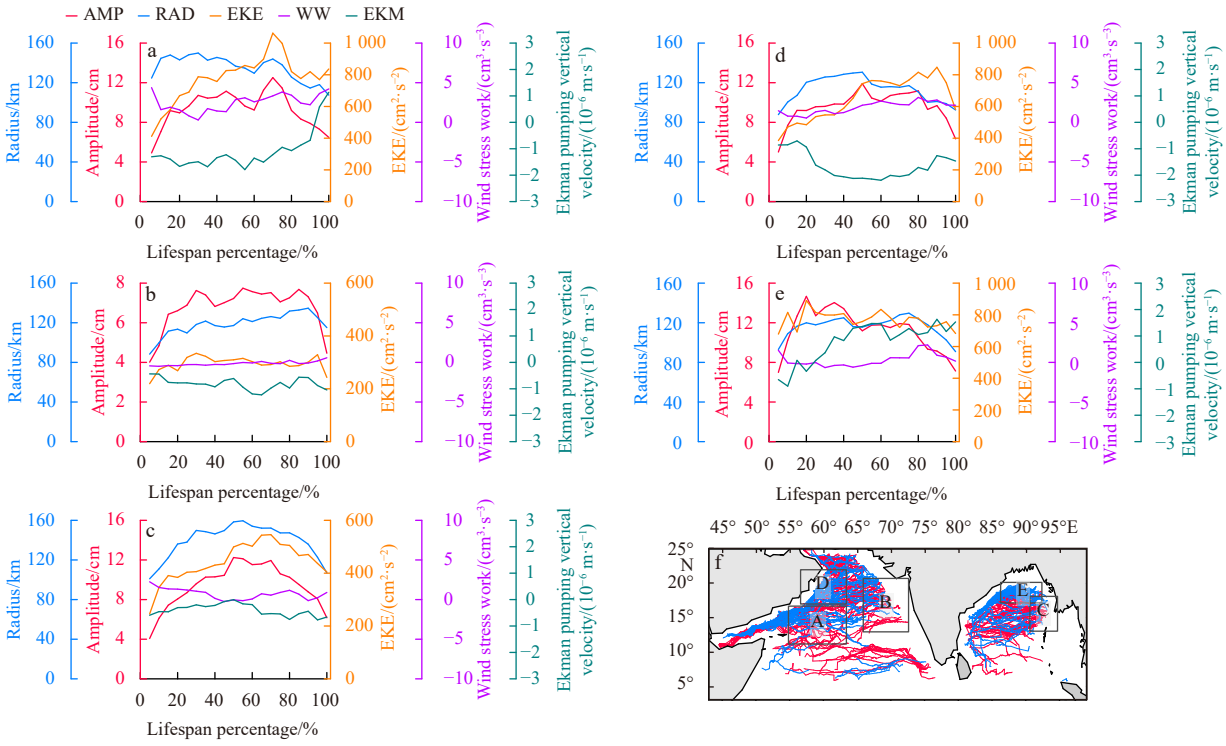

Fig. 15. The evolution characteristics of long lifespan eddies in the North Indian Ocean. a, b and c refer to AEs generated in Regions A, B, C in diagram f; d and e refer to CEs generated in Regions D, E in diagram f. AMP, RAD, EKE, WW and EKM refer to amplitude, radius, eddy kinetic energy, the wind stress work and the Ekman pumping vertical velocity, respectively.

of Sri Lanka propagate westward and generate Kelvin waves at the southeast of Sri Lanka, which travel across the southern tip of India together with the downwelling coastal Kelvin waves generated from BOB. These waves significantly increase the SSHA of Laccadive High, and derive these long lifespan AEs which propagate westward under the drive of the Northeast Monsoon Current. Besides, durable AEs also generate in the EAC region. These AEs mainly exist from April to July until the EAC turns northeastward and halts the westward propagation (Figs 13a and b).

CEs with long lifespan are relatively concentrated at the northwest part of AS (Figs 13g and h). These CEs are affected by the upwelling Kelvin waves along the coast of Arabia according to the study of Valsala and Rao (2016). Meanwhile, the radiated Rossby waves from the west coast of India (present as the negative SSHA band in Fig. 14a) are also crucial. These upwelling Rossby waves are radiated from the Kelvin waves along the east coast of India (show as negative SSHA band in Fig. 14c), which are raised by wind forcing to the east of Sri Lanka since August (Suresh et al., 2016). Besides, the instabilities caused by the southwestward EAC may also benefit these eddies. During normalized lifespan (Fig. 15d), the amplitude and radius increase in the first half of lifespan, and decrease in the rest half. The EKE increases in beginning 90% lifespan, and deceases in last 10% lifespan. The WW is 1.87 cm^3/s^3 on average, showing enhanced effect on CEs. However, the Ekman pumping vertical velocity is negative, indicating that the Ekman pumping process is not conducive to maintain these CEs.

In the BOB, long lifespan AEs are mostly formed near the west of Myanmar from June to January (Figs 13b–d). The downwelling coastal Kelvin waves dominate the coastal rim of BOB from June–August and October–December (Rao et al., 2010), which benefit the generation of these AEs, and the nonlinearity caused by Myanmar bump also promotes these eddies (Cheng et al., 2018). As shown in Fig. 15c, the amplitude, radius and EKE of these AEs have similar trends, increasing for the first half lifespan and decreasing for the rest period. The WW is 0.72 cm^3/s^3 on average. The Ekman pumping vertical velocity is -0.47×10^{-6} m/s on average, which is in favor of the maintenance of these AEs.

Durable CEs are concentrated in the north and northwest regions of BOB. These CEs are triggered by the upwelling coastal Kelvin waves, which propagate along the north boundary from January–April and August–September (Rao et al., 2010). Besides, the instability caused by northeastward EICC is also crucial from March to May. In addition, the radiated upwelling Rossby waves have effects on the CEs at northwest of BOB from September–December (present as negative SSHA band in Fig 14b). During the lifespan, the amplitude and EKE of these CEs increase at the starting 20% stage, and then gradually decrease (Fig. 15e). The WW is small, which is only 0.31 cm^3/s^3 on average. Whereas the Ekman pumping vertical velocity is larger with average value of 0.78×10^{-6} m/s, illustrating that the upwelling processes favor these CEs.

4 Conclusions

Adopting satellite altimeter data from 1993 to 2019, this study investigates the statistical characteristics of mesoscale eddies in the North Indian Ocean based on 1 800 AEs (1 500 CEs) in the AS and 776 AEs (878 CEs) in the BOB. These eddies mainly concentrate in the west or north regions of AS and BOB, which results in higher eddy frequency. The polarity of eddy reveals a zonal band distribution pattern in the AS, while the distribution of polarity is closely related to boundary geometry in the BOB.

As for the statistical characteristics, 51.8% (41.4%) of AEs (CEs) in the AS, and 45.8% (39.2%) AEs (CEs) in the BOB last longer than 50 days. Eddy lifespan increases with rising latitude, and then reduces as the basin narrow down at higher latitudes. Eddy radius mainly varies from 60 (70) to 180 km in the AS (BOB) and decreases with ascending latitude in both basins. The average zonal propagation speed of eddies is –8.37 (–8.26) cm/s for AEs (CEs) in the AS, while it is –8.01 (–8.24) cm/s in the BOB. Besides, the average meridional propagation speed of eddies is –0.63 (–0.62) cm/s for AEs (CEs) in the AS and –0.83 (–0.71) cm/s for AEs (CEs) in the BOB.

The seasonal variations of eddy characteristics are evident in the AS. Affected by the Kelvin waves along the west coast of India and radiated Rossby waves during the winter monsoon, more eddies generate during this period, while fewer eddies form during the summer monsoon. The AEs (CEs) emerged before the summer (winter) monsoon have longer lifespan. The EKE of AEs (CEs) is larger during the summer (winter) monsoon, due to the effects of seasonal wind and currents. The seasonal variation of the EKE mainly appears along the west boundary of AS, especially in the SC region. Furthermore, the Kelvin waves induced by wind forcing to the east of Sri Lanka could affect the EKE at the Laccadive Sea during the monsoon seasons. In the BOB, the characteristics of eddies are affected by seasonal wind and current, as well as intraseasonal instability caused by Kelvin waves and Rossby waves. Since the upwelling and downwelling Kelvin waves occur alternatively, more CEs generate in February–May and September–November, while more AEs form in June–August and December–January. AEs (CEs) generated before the arrival of the first downwelling (second upwelling) Kelvin waves have longer lifespan. The EKE of AEs and CEs peaks in April and May, owing to the enormous energy converted from the instabilities, which are generated by the first upwelling coastal Kelvin waves, the second downwelling Rossby waves radiated from the eastern boundary last year, and strong EICC. Meanwhile, large EKE occurs to the east of Sri Lanka from June to September, which is induced by the forcing of local wind stress. From November to December, EKE is larger along the east coast of India, as a result of the instability caused by southward EICC and the second downwelling coastal Kelvin waves. Additionally, the influence of wind stress work on EKE is further studied. The WW could enhance the EKE along the west boundary of AS during the two monsoon seasons, whereas the WW only has strong impact along the east coast of India in November and December. Moreover, the WW also exerts positive effects on EKE around the southern tip of India and southeast of Sri Lanka during the monsoon seasons.

Eventually, eddies with lifespan more than 100 days are further studied based on 241 AEs (171 CEs) in the AS and 78 AEs (64 CEs) in the BOB. In the AS, long lifespan AEs mainly generate in three regions: the Socotra, WICC and EAC regions, while durable CEs are concentrated at the northwest of AS. AEs are created at north of Socotra after GW collided with the Socotra Island, while long lifespan AEs at the east of Socotra are initiated by the Rossby waves radiated from the east boundary. AEs formed in the WICC region are triggered by the downwelling Kelvin waves from the BOB. Besides, the long lifespan AEs and CEs emerged at the northwest of AS are affected by the instability of Kelvin waves along the Arabia coast, Rossby waves radiated from the east basin, and the seasonal EAC. In the BOB, long lifespan AEs are mostly formed near the west of Myanmar, which are affected by the downwelling coastal Kelvin waves and the nonlinearity caused by the Myanmar bump. Durable CEs are accumulated at the north and northwest basin. The upwelling coastal Kelvin

waves, the radiated Rossby waves and the EICC exert enormous efforts on the formation of these eddies. Among the long lifespan eddies, AEs generated in the Socotra region have the largest EKE of 780 cm^2/s^2 on average, and CEs formed in the northwest region of BOB have larger EKE of 760 cm^2/s^2 on average.

Acknowledgements

The satellite altimeter data are produced by Ssalto/Duacs and distributed by CMEMS (https://www.resources.marine.copernicus.eu/products). The Cross-Calibrated Multi-Platform wind data are produced and distributed by RSS (http://www.remss.com/measurements/ccmp/).

References

Akuetevi C Q C, Barnier B, Verron J, et al. 2016. Interactions between the Somali Current eddies during the summer monsoon: Insights from a numerical study. Ocean Science, 12(1): 185–205, doi: 10.5194/os-12-185-2016

Al Saafani M A, Shenoi S S C, Shankar D, et al. 2007. Westward movement of eddies into the Gulf of Aden from the Arabian Sea. Journal of Geophysical Research: Oceans, 112(C11): C11004, doi: 10.1029/2006JC004020

Atlas R, Hoffman R N, Ardizzone J, et al. 2011. A cross-calibrated, multiplatform ocean surface wind velocity product for meteorological and oceanographic applications. Bulletin of the American Meteorological Society, 92(2): 157–174, doi: 10.1175/2010BAMS2946.1

Babu M T, Sarma Y V B, Murty V S N, et al. 2003. On the circulation in the Bay of Bengal during northern spring inter-monsoon (March–April 1987). Deep Sea Research Part II: Topical Studies in Oceanography, 50(5): 855–865, doi: 10.1016/S0967-0645(02)00609-4

Beal L M, Donohue K A. 2013. The Great Whirl: Observations of its seasonal development and interannual variability. Journal of Geophysical Research: Oceans, 118(1): 1–13, doi: 10.1029/2012JC008198

Beal L M, Hormann V, Lumpkin R, et al. 2013. The response of the surface circulation of the Arabian Sea to monsoonal forcing. Journal of Physical Oceanography, 43(9): 2008–2022, doi: 10.1175/JPO-D-13-033.1

Bruce J G, Johnson D R, Kindle J C. 1994. Evidence for eddy formation in the eastern Arabian Sea during the northeast monsoon. Journal of Geophysical Research: Oceans, 99(C4): 7651–7664, doi: 10.1029/94JC00035

Cai Yi, Li Hai. 2011. Study on the relationship between ENSO and tropical Indian Ocean temperature. Marine Science Bulletin, 13(1): 1–9

Chaigneau A, Eldin G, Dewitte B. 2009. Eddy activity in the four major upwelling systems from satellite altimetry (1992–2007). Progress in Oceanography, 83(1–4): 117–123, doi: 10.1016/j.pocean.2009.07.012

Chaigneau A, Gizolme A, Grados C. 2008. Mesoscale eddies off Peru in altimeter records: Identification algorithms and eddy spatio-temporal patterns. Progress in Oceanography, 79(2–4): 106–119, doi: 10.1016/j.pocean.2008.10.013

Chaigneau A, Pizarro O. 2005. Eddy characteristics in the eastern South Pacific. Journal of Geophysical Research: Oceans, 110(C6): C06005

Chatterjee A, Shankar D, McCreary J P, et al. 2017. Dynamics of Andaman Sea circulation and its role in connecting the equatorial Indian Ocean to the Bay of Bengal. Journal of Geophysical Research: Oceans, 122(4): 3200–3218, doi: 10.1002/2016JC012300

Chelton D. 2013. Mesoscale eddy effects. Nature Geoscience, 6(8): 594–595, doi: 10.1038/ngeo1906

Chelton D B, Gaube P, Schlax M G, et al. 2011a. The influence of nonlinear mesoscale eddies on near-surface oceanic chlorophyll. Science, 334(6054): 328–332, doi: 10.1126/science.1208897

Chelton D B, Schlax M G, Samelson R M. 2011b. Global observations of nonlinear mesoscale eddies. Progress in Oceanography, 91(2): 167–216, doi: 10.1016/j.pocean.2011.01.002

Chen Jiajia, Cheng Xuhua, Chen Xiao. 2019. Eddy generation mechanism in the eastern South China Sea. Acta Oceanologica Sinica, 38(4): 20–28, doi: 10.1007/s13131-019-1409-3

Chen Gengxin, Li Yuanlong, Xie Qiang, et al. 2018. Origins of eddy kinetic energy in the Bay of Bengal. Journal of Geophysical Research: Oceans, 123(3): 2097–2115, doi: 10.1002/2017JC013455

Chen Gengxin, Wang Dongxiao, Hou Yijun. 2012. The features and interannual variability mechanism of mesoscale eddies in the Bay of Bengal. Continental Shelf Research, 47: 178–185, doi: 10.1016/j.csr.2012.07.011

Cheng Xuhua, McCreary J P, Qiu Bo, et al. 2018. Dynamics of eddy generation in the Central Bay of Bengal. Journal of Geophysical Research: Oceans, 123(9): 6861–6875, doi: 10.1029/2018JC014100

Cheng Xuhua, Xie Shangping, McCreary J P, et al. 2013. Intraseasonal variability of sea surface height in the Bay of Bengal. Journal of Geophysical Research: Oceans, 118(2): 816–830, doi: 10.1002/jgrc.20075

Cui Wei, Yang Jungang, Ma Yi. 2016. A statistical analysis of mesoscale eddies in the Bay of Bengal from 22–year altimetry data. Acta Oceanologica Sinica, 35(11): 16–27, doi: 10.1007/s13131-016-0945-3

Dandapat S, Chakraborty A. 2016. Mesoscale eddies in the western Bay of Bengal as observed from Satellite Altimetry in 1993–2014: Statistical Characteristics, variability and three-dimensional properties. IEEE Journal of Selected Topics in Applied Earth Observations and Remote Sensing, 9(11): 5044–5054, doi: 10.1109/JSTARS.2016.2585179

Dong Di, Brandt P, Chang Ping, et al. 2017. Mesoscale eddies in the northwestern Pacific Ocean: Three-dimensional eddy structures and heat/salt transports. Journal of Geophysical Research: Oceans, 122(12): 9795–9813, doi: 10.1002/2017JC013303

Dong Changming, McWilliams J C, Liu Yu, et al. 2014. Global heat and salt transports by eddy movement. Nature Communications, 5(1): 3294, doi: 10.1038/ncomms4294

Ducet N, Le Traon P Y, Reverdin G. 2000. Global high-resolution mapping of ocean circulation from TOPEX/Poseidon and ERS-1 and -2. J. Journal of Geophysical Research: Oceans, 105(C8): 19477–19498, doi: 10.1029/2000JC900063

Fischer J, Schott F, Stramma L. 1996. Currents and transports of the Great Whirl-Socotra Gyre system during the summer monsoon, August 1993. Journal of Geophysical Research: Oceans, 101(C2): 3573–3587, doi: 10.1029/95JC03617

Fratantoni D M, Bower A S, Johns W E, et al. 2006. Somali Current rings in the eastern Gulf of Aden. Journal of Geophysical Research:Oceans, 111(C9): C09039

Frenger I, Gruber N, Knutti R, et al. 2013. Imprint of Southern Ocean eddies on winds, clouds and rainfall. Nature Geoscience, 6(8): 608–612, doi: 10.1038/ngeo1863

Geng Wu, Xie Qiang, Chen Gengxin, et al. 2016. Numerical study on the eddy–mean flow interaction between a cyclonic eddy and Kuroshio. Journal of Oceanography, 72(5): 727–745, doi: 10.1007/s10872-016-0366-0

Han Weiqing, McCreary J P Jr. 2001. Modeling salinity distributions in the Indian Ocean. Journal of Geophysical Research: Oceans, 106(C1): 859–877, doi: 10.1029/2000JC000316

Hu Zifeng, Tan Yehui, Song Xingyu, et al. 2014. Influence of mesoscale eddies on primary production in the South China Sea during spring inter-monsoon period. Acta Oceanologica Sinica, 33(3): 118–128, doi: 10.1007/s13131-014-0431-8

Ivchenko V O, Tréguier A M, Best S E. 1997. A kinetic energy budget and internal instabilities in the Fine Resolution Antarctic Model. Journal of Physical Oceanography, 27(1): 5–22, doi: 10.1175/1520-0485(1997)027<0005:AKEBAI>2.0.CO;2

Li Jiaxun, Zhang Ren, Liu Chenzhao, et al. 2012. Modeling of ocean mesoscale eddy and its application in the underwater acoustic propagation. Marina Science Bulletin, 14(1): 1–15

Ma Jing, Xu Haiming, Dong Changming. 2016. Seasonal variations in atmospheric responses to oceanic eddies in the Kuroshio Extension. Tellus A: Dynamic Meteorology and Oceanography, 68(1): 31563, doi: 10.3402/tellusa.v68.31563

Mason P J, Sykes R I. 1978. On the interaction of topography and Ekman boundary layer pumping in a stratified atmosphere. Quarterly Journal of the Royal Meteorological Society, 104(440): 475–490, doi: 10.1002/qj.49710444018

Morrow R, Birol F, Griffin D, et al. 2004. Divergent pathways of cyclonic and anti-cyclonic ocean eddies. Geophysical Research Letters, 31(24): L24311, doi: 10.1029/2004GL020974

Okubo A. 1970. Horizontal dispersion of floatable particles in the vicinity of velocity singularities such as convergences. Deep-Sea Research and Oceanographic Abstracts, 17(3): 445–454, doi: 10.1016/0011-7471(70)90059-8

Penven P, Echevin V, Pasapera J, et al. 2005. Average circulation, seasonal cycle, and mesoscale dynamics of the Peru Current System: A modeling approach. Journal of Geophysical Research: Oceans, 110(C10): C10021, doi: 10.1029/2005JC002945

Prasad T G, Ikeda M. 2001. Spring evolution of Arabian Sea high in the Indian Ocean. Journal of Geophysical Research: Oceans, 106(C12): 31085–31098, doi: 10.1029/2000JC000314

Rao R R, Girish Kumar M S, Ravichandran M, et al. 2010. Interannual variability of Kelvin wave propagation in the wave guides of the equatorial Indian Ocean, the coastal Bay of Bengal and the southeastern Arabian Sea during 1993–2006. Deep-Sea Research Part I: Oceanographic Research Papers, 57(1): 1–13, doi: 10.1016/j.dsr.2009.10.008

Sadarjoen I A, Post F H. 1999. Geometric methods for vortex extraction. In: Data Visualization'99. Vienna: Springer, 53–62

Sadarjoen I A, Post F H. 2000. Detection, quantification, and tracking of vortices using streamline geometry. Computers & Graphics, 24(3): 333–341

Schott F A, McCreary J P. 2001. The monsoon circulation of the Indian Ocean. Progress in Oceanography, 51(1): 1–123, doi: 10.1016/S0079-6611(01)00083-0

Shankar D, Shetye S R. 1997. On the dynamics of the Lakshadweep high and low in the southeastern Arabian Sea. Journal of Geophysical Research: Oceans, 102(C6): 12551–12562, doi: 10.1029/97JC00465

Shankar D, Vinayachandran P N, Unnikrishnan A S. 2002. The monsoon currents in the North Indian Ocean. Progress in Oceanography, 52(1): 63–120, doi: 10.1016/S0079-6611(02)00024-1

Sreenivas P, Gnanaseelan C, Prasad K V S R. 2012. Influence of El Niño and Indian Ocean Dipole on sea level variability in the Bay of Bengal. Global and Planetary Change, 80–81: 215–225

Sun Jia, Wang Guihua, Xiong Xuejun, et al. 2020. Impact of warm mesoscale eddy on tropical cyclone intensity. Acta Oceanologica Sinica, 39(8): 1–13, doi: 10.1007/s13131-020-1617-x

Suresh I, Vialard J, Izumo T, et al. 2016. Dominant role of winds near Sri Lanka in driving seasonal sea level variations along the west coast of India. Geophysical Research Letters, 43(13): 7028–7035, doi: 10.1002/2016GL069976

Suresh I, Vialard J, Lengaigne M, et al. 2013. Origins of wind-driven intraseasonal sea level variations in the North Indian Ocean coastal waveguide. Geophysical Research Letters, 40(21): 5740–5744, doi: 10.1002/2013GL058312

Tong Kai, Liu Jinfang, Yan Ming, et al. 2003. Space-time characteristic analysis of wind field over the south Indian Ocean. Marine Science Bulletin, 5(2): 5–13

Trott C B, Subrahmanyam B, Chaigneau A, et al. 2018. Eddy tracking in the northwestern Indian Ocean during southwest monsoon regimes. Geophysical Research Letters, 45(13): 6594–6603, doi: 10.1029/2018GL078381

Valsala V K, Rao R R. 2016. Coastal Kelvin waves and dynamics of Gulf of Aden eddies. Deep-Sea Research Part I: Oceanographic Research Papers, 116: 174–186, doi: 10.1016/j.dsr.2016.08.003

Vic C, Roullet G, Carton X, et al. 2014. Mesoscale dynamics in the Arabian Sea and a focus on the Great Whirl life cycle: A numerical investigation using ROMS. Journal of Geophysical Research: Oceans, 119(9): 6422–6443, doi: 10.1002/2014JC009857

Weiss J. 1991. The dynamics of enstrophy transfer in two-dimensional hydrodynamics. Physica D: Nonlinear Phenomena, 48(2–3): 273–294, doi: 10.1016/0167-2789(91)90088-Q

Wentz F J, Scott J, Hoffman R, et al. 2015. Remote sensing systems cross-calibrated multi-platform (CCMP) 6-hourly ocean vector wind analysis product on 0.25 deg grid, version 2.0. Santa Rosa, CA: Remote Sensing Systems

Willett C S, Leben R R, Lavín M F. 2006. Eddies and tropical instability waves in the eastern tropical Pacific: A review. Progress in Oceanography, 69(2–4): 218–238, doi: 10.1016/j.pocean.2006.03.010

Yang Guang, Wang Fan, Li Yuanlong, et al. 2013. Mesoscale eddies in the northwestern subtropical Pacific Ocean: Statistical characteristics and three-dimensional structures. Journal of Geophysical Research: Oceans, 118(4): 1906–1925, doi: 10.1002/jgrc.20164

Yang Guang, Yu Weidong, Yuan Yeli, et al. 2015. Characteristics, vertical structures, and heat/salt transports of mesoscale eddies in the southeastern tropical Indian Ocean. Journal of Geophysical Research: Oceans, 120(10): 6733–6750, doi: 10.1002/2015JC011130

Zhang Zhiwei, Tian Jiwei, Qiu Bo, et al. 2016. Observed 3D structure, generation, and dissipation of oceanic mesoscale eddies in the South China Sea. Scientific Reports, 6(1): 24349, doi: 10.1038/srep24349

Zhang Zhengguang, Wang Wei, Qiu Bo. 2014a. Oceanic mass transport by mesoscale eddies. Science, 345(6194): 322–324, doi: 10.1126/science.1252418

Zhang Zhiwei, Zhong Yisen, Tian Jiwein, et al. 2014b. Estimation of eddy heat transport in the global ocean from Argo data. Acta Oceanologica Sinica, 33(1): 42–47, doi: 10.1007/s13131-014-0421-x

Zu Tingting, Wang Dongxiao, Yan Changxiang, et al. 2013. Evolution of an anticyclonic eddy southwest of Taiwan. Ocean Dynamics, 63(5): 519–531, doi: 10.1007/s10236-013-0612-6